The EMBO Journal vol.15 no.7 pp.1515–1523, 1996

Structure of a neutralizing antibody bound bivalently to human rhinovirus 2

Elizabeth A.Hewat[1] and Dieter Blaas[2]

Institut de Biologie Structurale Jean-Pierre Ebel, 41 Avenue des Martyrs, Grenoble, France and [2]Institute of Biochemistry, University of Vienna, Dr Bohr Gasse 9/3, A-1030 Vienna, Austria

[1]Corresponding author

The structure of a complex between human rhinovirus serotype 2 (HRV2) and the weakly neutralizing monoclonal antibody 8F5 has been determined to 25 Å resolution by cryo-electron microscopy and 3-D reconstruction techniques. The antibody is seen to be bound bivalently across the icosahedral 2-fold axis, despite the very short distance of 60 Å between the symmetry-related epitopes. The canyon around the 5-fold axis is not obstructed. Due to extreme flexibility of the hinge region the Fc domains occupy random orientations and are not visible in the reconstruction. The atomic coordinates of Fab-8F5 complexed with a synthetic peptide derived from the viral protein 2 (VP2) epitope were fitted to the structure obtained by cryo-electron microscope techniques. The X-ray structure of HRV2 is not known, so that of the closely related HRV1A was placed in the electron microscopic density map. The footprint of 8F5 on the viral surface is largely on VP2, but also covers the VP3 loop centred on residue 3060. C_α atoms of VP1 and 8F5 come no closer than 10 Å. Based on the fit of the X-ray coordinates to the electron microscope data, the synthetic 15mer peptide starts and ends in close proximity to the corresponding amino acids of VP2 on HRV1A. However, the respective loops diverge considerably in their overall spatial disposition. It appears from this study that bivalent binding of an antibody directed against a picornavirus exists for a smaller spanning distance than was previously thought possible. Also bivalent binding does not ensure strong neutralization.

Keywords: cryo-electron microscopy/image analysis/ HRV2/mAb 8F5/virus neutralization

Introduction

Human rhinoviruses (HRVs), members of the picornavirus family, are a major cause of the common cold. They are icosahedral RNA viruses, 300 Å in diameter, and are composed of 60 copies each of four viral coat proteins VP1, VP2, VP3 and VP4, on a $T = 1$ icosahedral lattice (Rossmann *et al.*, 1985). The viruses exhibit vast antigenic variation with over 100 serotypes currently identified. With one exception they are classified into either a major or a minor group based on their specificity for cell receptors: intercellular adhesion molecule 1 (ICAM-1) for the major group (Greve *et al.*, 1989; Staunton *et al.*, 1989; Tomassini *et al.*, 1989) and members of the low density lipoprotein receptor (LDL-R) family for the minor group (Hofer *et al.*, 1994). The recognition site of ICAM-1 in the canyon [a cleft encircling the 5-fold axis of symmetry (Rossmann *et al.*, 1985)] was recently determined by cryo-electron microscopy and X-ray crystallography techniques (Olson *et al.*, 1993) thus confirming the canyon hypothesis (Rossmann, 1989). The binding site of the LDL receptors is not known at present. Comparison of surface properties of major and minor group viruses (Chapman and Rossmann, 1993) and results of site-directed mutagenesis experiments suggest that it is not identical to the ICAM-1 binding site (Duechler *et al.*, 1993).

The antigenic properties of picornaviruses and of HRVs in particular have been extensively studied. However, our understanding of the molecular mechanisms of viral neutralization by antibodies is still limited. The binding sites for neutralizing antibodies are generally located on loops which decorate the viral surface. These loops, not surprisingly, contain the least conserved sequences between serotypes. The study of escape mutants to neutralization by monoclonal antibodies (mAbs) has led to the definition of four neutralizing immunogenic sites (NIm-IA, NIm-IB, NIm-II, and NIm-III) for the major group virus HRV14 (Sherry *et al.*, 1985) and three such sites designated A, B and C for the minor group virus HRV2 (Appleyard *et al.*, 1990). Several different mechanisms of viral neutralization are known to exist and any given antibody may invoke a subtle mixture to these mechanisms. For example, viral infectivity may be neutralized by viral aggregation as a result of interlinking of particles, by inhibition of virus receptor binding, or by inhibition of virus uncoating (Mosser *et al.*, 1989). An important element in understanding virus neutralization is the knowledge of virus/antibody structures for a range of antibodies with different neutralizing properties. Cryo-electron microscopy and 3-D reconstruction have already demonstrated their value in this field (Prasad *et al.*, 1990; Trus *et al.*, 1992) and when combined with X-ray crystallographic data of the constituent elements (virus and/or Fab) a more complete picture of the virus/Fab interface at a resolution of 5 Å is obtained (Wang *et al.*, 1992; Porta *et al.*, 1994; Wikoff *et al.*, 1994). In particular, the most detailed view of a virus/Fab interface known to date is that obtained by combined cryo-electron microscopy and X-ray techniques for HRV14 complexed with the strongly neutralizing mAb17-IA (Smith *et al.*, 1993a,b; Liu *et al.*, 1994). The mAb17-IA was shown to be bound bivalently to HRV14 and to largely obscure the receptor binding site. The area of the virus/Fab interaction is very large, and includes contacts with the variable domain of the heavy chain framework (Smith *et al.*, 1993b). This demonstration of bivalent binding of a strongly neutralizing antibody is in agreement with the hypothesis that bivalent binding confers strong neutralization by pre-

venting the dissociation of the adjacent pentamers (Mosser *et al.*, 1989). However, this particular antibody primarily prevents interaction with the receptors.

In the present investigation we have employed cryo-electron microscopy and 3-D reconstruction techniques combined with X-ray crystallographic data to study the structure of HRV2 complexed with the very weakly neutralizing mAb 8F5. The X-ray structure of both the Fab 8F5 and the Fab 8F5 complexed with a synthetic peptide, corresponding to a contiguous epitope on VP2 of HRV2, are both known (Tormo *et al.*, 1992, 1994). The X-ray structure of HRV2 is not known at present so the structure of the closely related HRV1A (Kim *et al.*, 1989), which has 73% amino acid sequence similarity of its capsid proteins, was used instead. Bivalent attachment of mAb 8F5 on HRV2 was predicted from the measured stoichiometry of binding and also from docking the X-ray structure of 8F5 Fab onto HRV1A (Tormo *et al.*, 1995). This prediction is essentially confirmed although the angle between the viral surface and the antibody was found to differ by about 30° from the structure obtained by model building.

Results and discussion

Cryo-electron microscopy of HRV2 and HRV2/8F5 complexes

In the cryo-electron microscope images native HRV2 particles appeared as smooth spheres with only slight surface texture discernible at high defocus. At high concentration they easily form hexagonal close packed rafts (Figure 1A). Observation of HRV2/Fab-8F5 complexes revealed that Fab molecules were only occasionally attached to the virus and thus were not suitable for further analysis (not shown). Due to the monovalency of the Fab fragment the avidity for HRV2 is apparently too low for stable association [see also Tormo *et al.* (1995)]. Cryo-electron microscope images of complexes between 8F5 IgG and HRV2 revealed high occupancy with a hedgehog-like appearance and there was no appreciable aggregation (Figure 1B). The background of unbound IgG which was present when mixtures of HRV2 and 8F5 IgG were observed without purification (not shown) was strongly reduced when excess mAb was removed by the use of spun columns. As in the native HRV2 specimen, a small proportion of the capsids was empty. They were also decorated with mAbs.

Reconstructed density of the HRV2/mAb-8F5 complex

The isosurface representations of the HRV2/mAb-8F5 complex corrected for the contrast transfer function, CTF, (Figure 2) show the HRV2 decorated with 60 bilobed Fabs which face each other across the icosahedral 2-fold axis. The effect of the CTF correction is not very noticeable in the isosurface representation but manifests itself most strongly at the 'necks' joining regions of density. The 'necks' tend to be thickened by the CTF correction (not shown). There is no evidence of density corresponding to the Fc domains. This can be explained by random orientations of the Fc domains with respect to the Fabs in agreement with previous observations (Wade *et al.*, 1989; Smith *et al.*, 1993a) which demonstrate the extreme

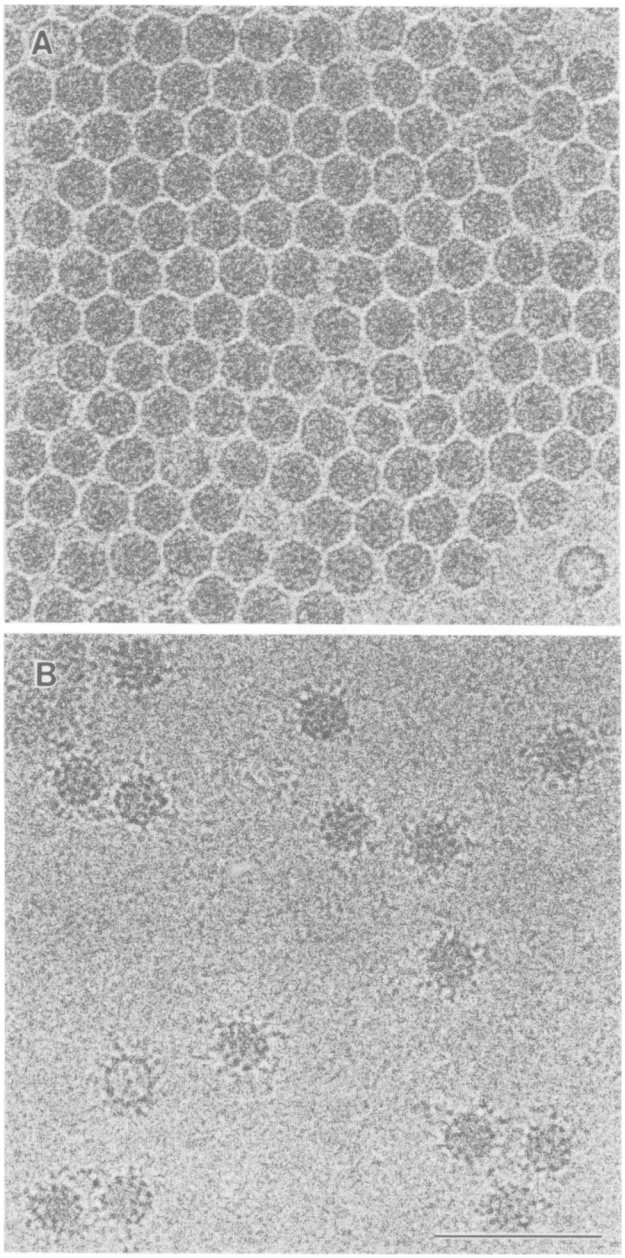

Fig. 1. Electron micrographs of frozen hydrated native HRV2 (**A**) and the HRV2/mAb-8F5 complex (**B**). The scale bar represents 1000 Å.

flexibility of the hinge. In the reconstruction, the maximum density in the Fab and in the viral capsid are the same, indicating an occupation of the virus with mAb of close to 100%. Most probably, particles with less than maximal occupancy were excluded from the reconstruction as they have less well-defined icosahedral symmetry. The density joining the pairs of Fab across the 2-fold axes is fairly weak and diffuse, again pointing to a higher flexibility in this region.

The isosurface representation of native HRV1A restricted to 25 Å resolution was calculated from the X-ray structure (Figure 3A) and is compared with an isosurface representation of the 25 Å reconstruction of HRV2 from the electron micrographs (Figure 3B). This representation was extracted from the reconstruction of the HRV2/mAb-8F5 complex by masking off all the

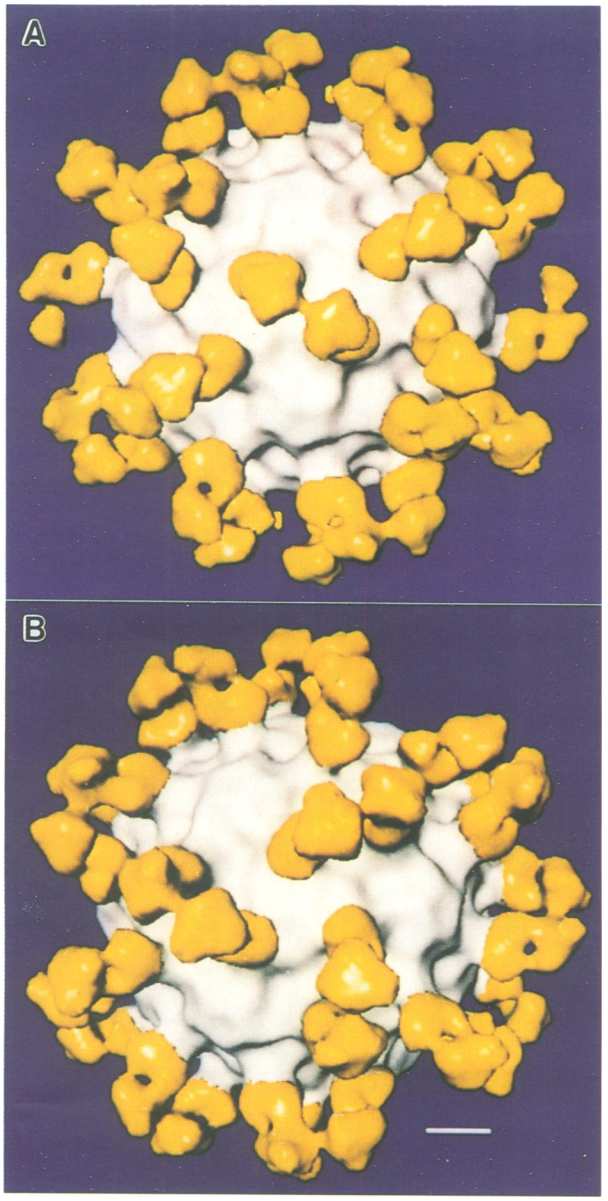

Fig. 2. Isosurface representations of the reconstructed HRV2/mAb-8F5 complex corrected for the CTF, viewed down a 2-fold axis (**A**) and a 3-fold axis (**B**). The HRV2 is coloured white (radius <160 Å) and the mAb-8F5 is coloured yellow (radius >160 Å). There is no visible density that could be attributed to the Fc fragment. Only the front half of the virus/8F5 complex is imaged. The scale bar represents 50 Å.

density beyond a radius of 160 Å and using a high threshold to eliminate the 'necks' between the capsid surface and the bound mAbs. The similarity of surface features of these closely related HRVs is manifest and both viruses strongly resemble HRV14 in a similar representation (Smith *et al.*, 1993a). A small difference is evident at the 8F5 binding site but this can be accounted for by interference from the 8F5 density in the imaging process. We cannot detect any real changes in the virion structure upon antibody binding. At this resolution the immunogenic loops are seen as small protrusions on the surface. The three HRVs exhibit the same topology, i.e. a pentameric dome on each of the icosahedral 5-fold axes surrounded by the 'canyon' with a raised triangular plateau centred on each of the icosahedral 3-fold axes. The hand of the electron microscope reconstruction was based on comparison with the X-ray enantiomorphic features. This hand was also confirmed by the enantiomorphic features of the X-ray structure of the 8F5 Fab.

Fit of X-ray structures of the Fab 8F5 and HRV1A to the cryo-electron microscope reconstructed density

In principle, the fit of an Fab structure into a 25 Å resolution map can be made in two orientations related by a 180° rotation about the long (pseudodyad) axis of the antibody fragment. In the case of 8F5, the fit of the Fab X-ray structure to the reconstructed density of the HRV2/8F5 mAb complex was facilitated by the knowledge of the structure of the complex between the Fab 8F5 and the synthetic peptide corresponding to the contiguous epitope at the puff between βE and αB of VP2 of HRV2 (Kim *et al.*, 1989; Tormo *et al.*, 1994). This is site B in HRV2 which is equivalent to the NIm-II site of HRV14 (Sherry *et al.*, 1985). The orientation of the Fab with respect to the viral capsid could thus be determined without ambiguity. The 150° elbow angle of the Fab 8F5 co-crystallized with the synthetic peptide also gave a unique orientation for the best fit in agreement with that predicted by the position of the peptide on the virus surface (Figures 3C and 4). The Fab elbow angle is defined as the angle between the two pseudodyad axes relating the heavy and light chain in the variable and constant modules. The Fab 8F5 (co-crystallized with the synthetic peptide) with an elbow angle of 150° fits the electron microscopic density map better than the uncomplexed Fab which has an elbow angle of 127°. The general fit is very good except at the elbow and on the distal end of the Fab (Figure 5A and B) where the map lacks a little density. This loss of density could possibly be explained by movement of the elbow associated with movement of the constant domain of the Fab.

The distance across the icosahedral 2-fold axis between the C-terminal (Arg 218) C_α of the cleaved heavy chains is 29 Å. This is consistent with a bivalent binding of the mAb and the hinge being on the 2-fold axis. The possibility that the reconstruction represents a monovalent attachment of the mAb with an additional 60 Fab to be accounted for in the noise is practically impossible because of the steric hindrance that would occur between the neighbouring mAbs across the 2-fold axis. The fit at the virus/Fab interface is particularly interesting (Figure 6). The 15mer synthetic peptide (white) and the corresponding amino acid sequence on VP2 of HRV1A (magenta), start and end close together but diverge considerably as they loop out from the virus capsid. Surprisingly, the carboxyl end of the synthetic peptide points towards the Fab rather than towards the virus capsid. While there is no sequence homology between these two immunogenic loops of VP2 on HRV2 and HRV1A, there is a strong sequence homology on either side of the loop. Given the remarkably good agreement between the basic structure of VP2 in HRV14, HRV1A and HRV16 except for the immunogenic loops (Rossmann *et al.*, 1985; Kim *et al.*, 1989; Oliveira *et al.*, 1993), there is good reason to believe that the immunogenic loops in question are anchored at both ends in a similar position and orientation. Thus, at least the disposition of the carboxyl end of the 15mer peptide

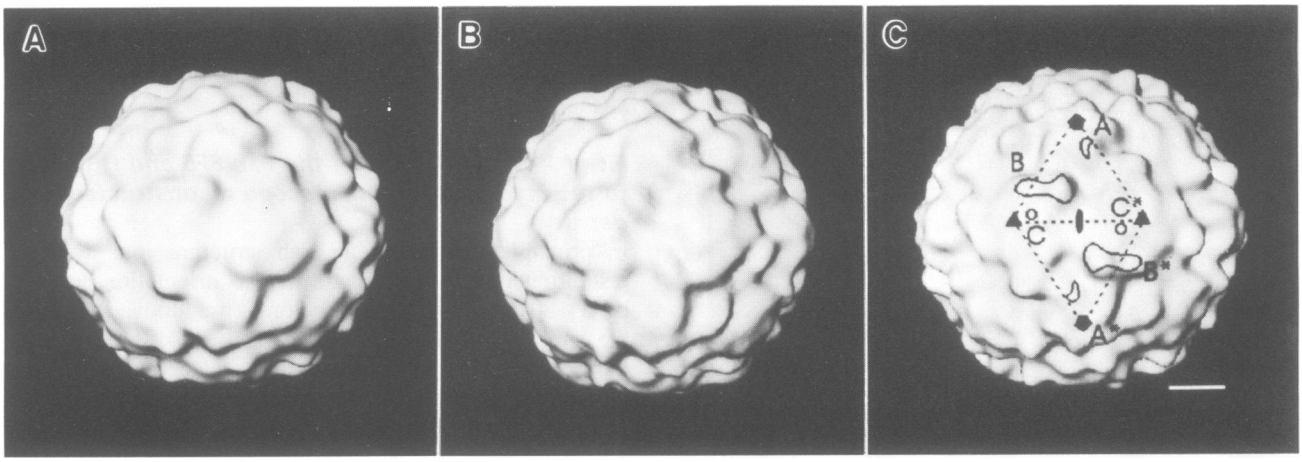

Fig. 3. Isosurface representations of the X-ray map of HRV1A (**A**) limited to 25 Å resolution, and the reconstructed cryo-electron microscopy map of HRV2 (**B**) to 25 Å resolution. The mAb-8F5 was masked off at a radius of 160 Å and a very high threshold applied. (**C**) Isosurface representation of the X-ray map of HRV1A limited to 20 Å resolution. Two asymmetric unit triangles and the known immunogenic sites of HRV2 are marked. One mAb 8F5 binds to sites B and B*. All representations are viewed down the 2-fold axis. The scale bar represents 50 Å.

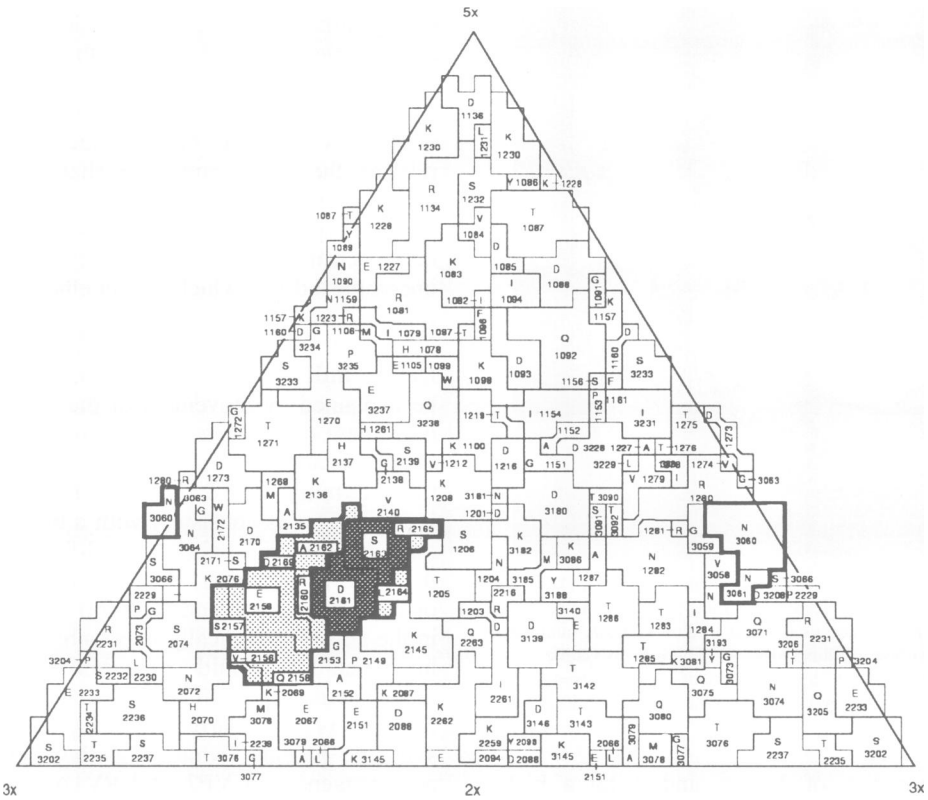

Fig. 4. Roadmap of HRV1A from Kim *et al.* (1989). The amino acids corresponding to the 15mer peptide of HRV2 which was co-crystallized with the mAb-8F5 are shaded grey and the two residues shaded a darker grey correspond to the residues in HRV2 which are involved in most of the contacts between 8F5 and the 15mer peptide (see Tormo *et al.*, 1994). The immunogenic loop on VP3 (C_αs closer than 5 Å) which interacts with the complementarity-determining-region CDR-L1 of 8F5 is outlined. The scale bar represents 100 Å.

adopted in the complex with 8F5 most probably differs from that of the corresponding one in HRV2. Without knowing the HRV2 atomic structure, it is impossible to decide whether the difference in structure reflects true differences in conformation between the antigenic loop in HRV2 and HRV1A or whether it is due to a rearrangement of the HRV2 loop induced by the bound mAb. 'Induced fit' of an antigenic loop as a consequence of antibody binding to polio virus was recently suggested following X-ray studies of a Fab fragment of C3 complexed with a peptide corresponding to the viral epitope (Wein *et al.*, 1995).

The 8F5 footprint is largely on VP2, the immunogenic loop corresponding to the 15mer peptide accounting for most of the contacts between mAb and viral capsid, with the notable exception of the CDR-L1 loop of 8F5 which interacts with the small immunogenic loop centred on residue 3060 of VP3. This loop on VP3 has been termed

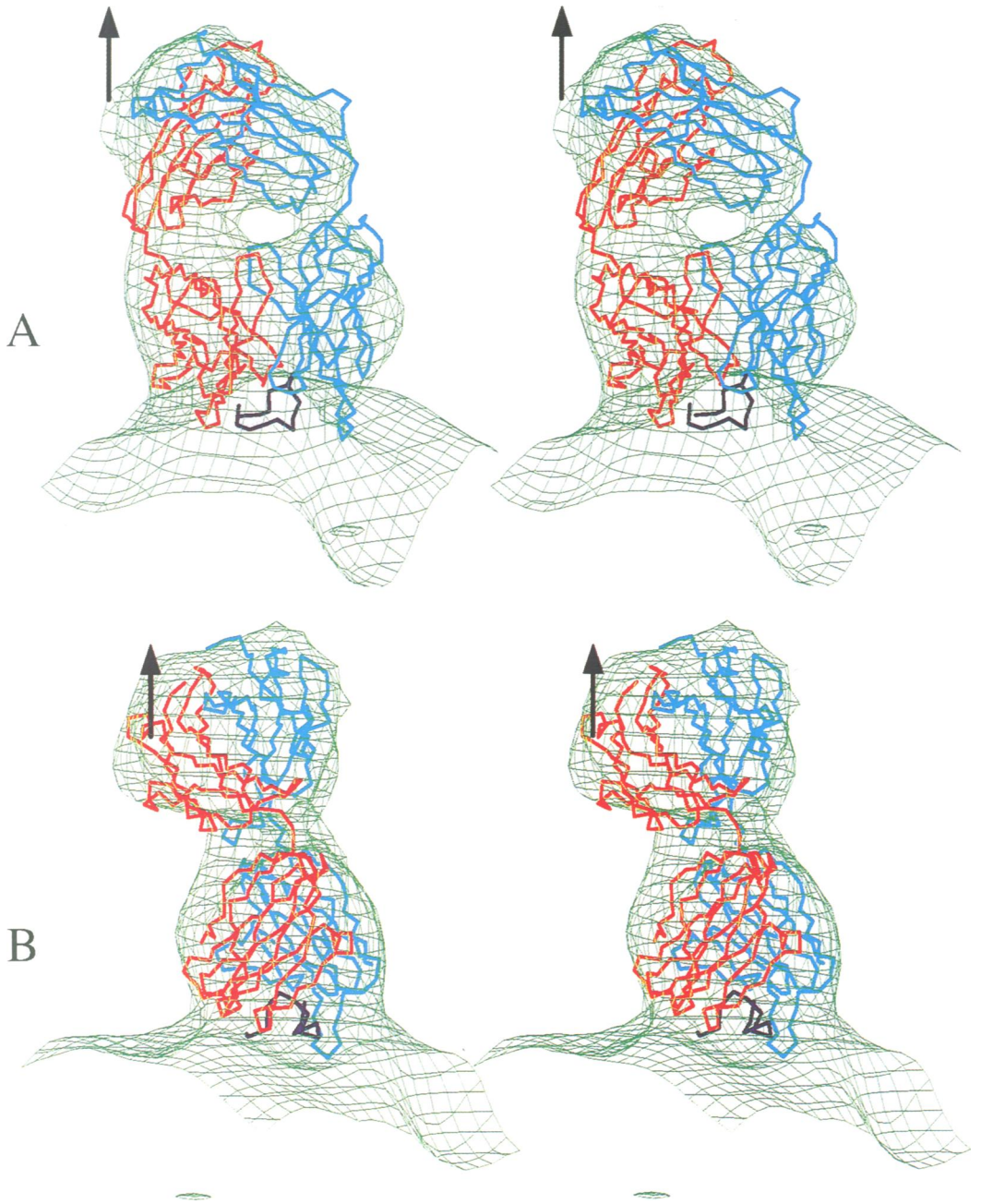

Fig. 5. Stereo views of the fit of the X-ray crystallographic structure of the Fab-8F5 (plus the 15mer synthetic peptide) into the cryo-electron microscope reconstruction of the HRV2/mAb-8F5 complex. The C_α backbones of the Fab-8F5 light chain and heavy chain are shown in blue and red respectively. The electron microscope map is depicted in green. The 15mer synthetic peptide is represented in dark blue. The 2-fold axis is indicated by an arrow in (**A**) and (**B**). In (**B**) the Fab is viewed from close to the 2-fold axis along the elbow. It will be noted that the small 'neck' of density connecting the Fabs across the 2-fold axis is most probably not the position of the hinge.

the VP3 'knob' (Rossmann *et al.*, 1985) and from studies with escape mutants it is known to be immunogenic on HRV2 (Appleyard *et al.*, 1990), whereas no such mutants have been detected for HRV14 (Sherry *et al.*, 1985). The polypeptide backbone of VP1 comes no closer than 10 Å to those of the antibody. In the absence of the HRV2 structure at atomic resolution, a more detailed analysis of the mAb-8F5/HRV2 interface is not possible.

The centre-to-centre distance between adjacent footprints across the 2-fold axes is ~60 Å (Figure 7). This is lower than the previously estimated minimal spanning distance of 70 Å (Mosser *et al.*, 1989). The extreme flexibility of the hinge region has already been invoked to explain the movement of the Fc domain with respect to the Fabs. It may equally well be used to account for this comparatively short spanning distance. The difference in affinity of the mAb 8F5 and the Fab 8F5 for HRV2 is consistent with the increased avidity of bivalent as compared with monovalent binding due to the effect of cooperativity (the mAb can dance with one foot in the air at a time and still keep hold). Also the Fab 8F5 apparently has a greater affinity for the 15mer synthetic peptide than for VP2 on the native HRV2. This is probably due, at least in part, to the relative flexibility of the peptide

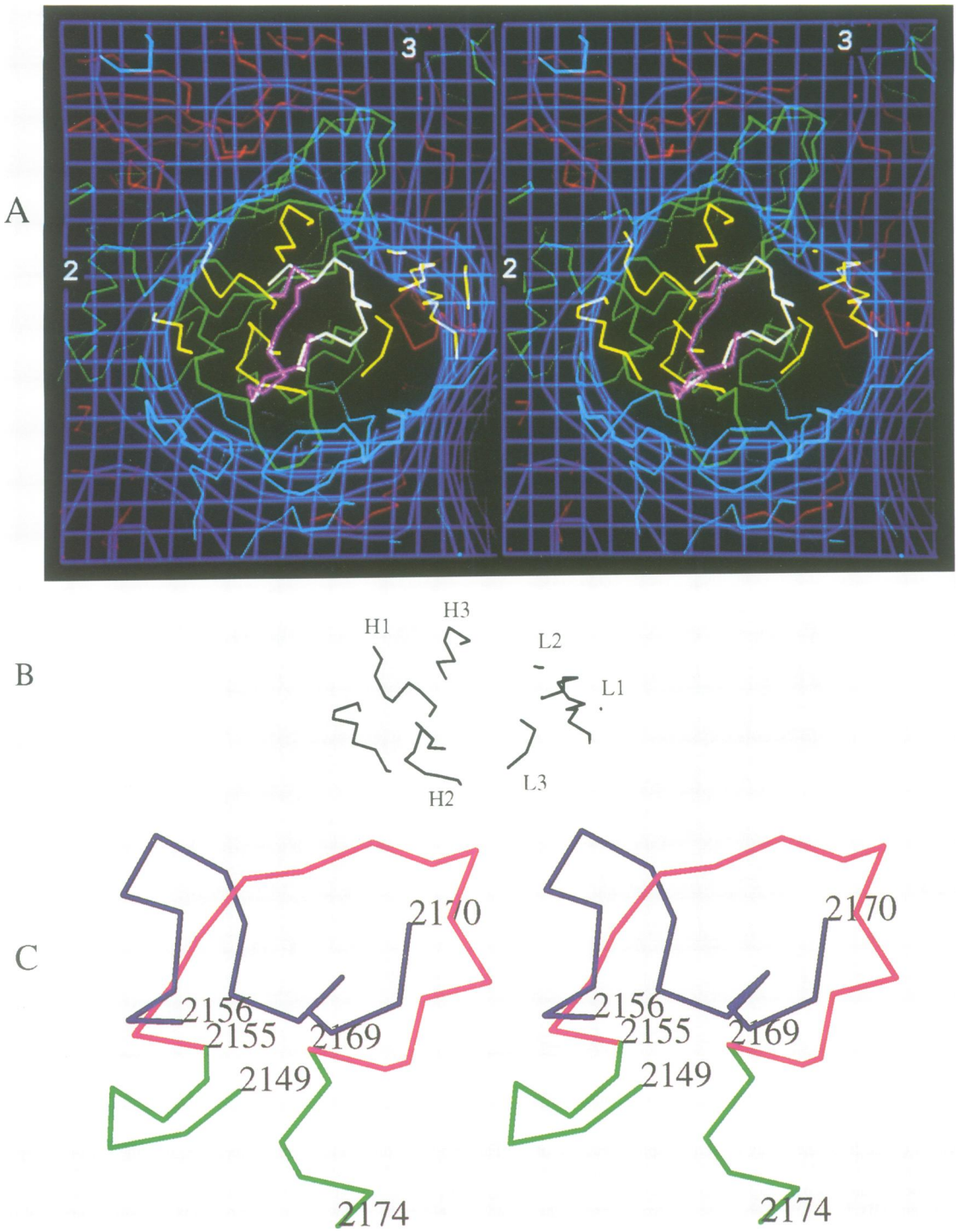

Fig. 6. (**A**) Stereo view of the footprint of 8F5 on HRV1A. The C_α backbones of VP1, VP2 and VP3 are coloured light blue, green and red respectively. The C_α backbones of the Fab-8F5 are shown in yellow. The electron microscope map is depicted in blue. The 15mer synthetic peptide is represented in white and the corresponding amino acids on VP2 of HRV1A are coloured magenta. The C_α backbone of 8F5 (CDR-L1) approaches to within 5 Å of the VP3 loop (red) centred on Asn3060 (identical in HRV1A and in HRV2). (Note: The first digit indicates the viral capsid protein, 1, 2, 3 or 4.) (**B**) A selection from (A) indicating the 8F5 Fab CDR loops. H indicates heavy chain and L light chain. The unmarked chain is part of the heavy chain. (**C**) The 15mer synthetic peptide (in dark blue) and the corresponding amino acids on VP2 of HRV1A (in magenta) start and end very close together but diverge considerably in their overall conformation. These chains are viewed from close to the icosahedral 2-fold axis.

in solution compared to the rigidity of the corresponding sequence on the virion which is anchored at both ends and constrained to a fixed conformation. The peptide is free to adopt the most suitable conformation to bind to the Fab and the area of contact may include the terminal residues of the peptide not normally involved in Fab/virion binding.

Comparison of the HRV2/mAb-8F5 reconstruction and the X-ray docking model

A model for the HRV2/8F5 complex has been proposed from docking of the Fab (complexed with the synthetic peptide derived from VP2 of HRV2) onto HRV1A (Tormo *et al.*, 1995). The conformation adopted by a 10 residue

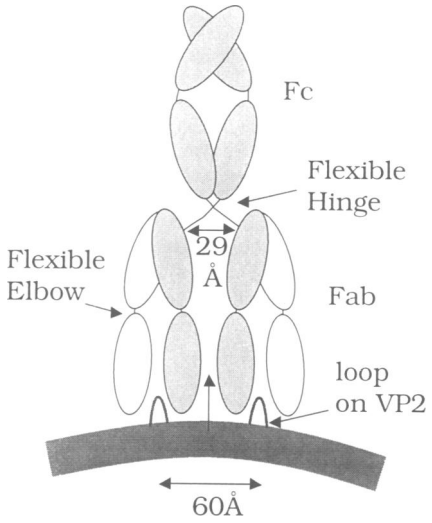

Fig. 7. Schematic drawing of the antibody bound to HRV2. The icosahedral 2-fold axis is marked in the centre of the drawing. Regions of the heavy chain are shaded in grey and the light chain in white.

long part of the peptide is similar to and could be superimposed onto the corresponding region of VP2 on HRV1A. This superposition was then used to place the Fab-8F5/peptide complex onto HRV1A. This docking procedure produced a model which predicted bivalent binding for 8F5 which has been confirmed by the current electron microscope study. There is, however, a considerable difference in the orientation of the Fab at the virus/Fab interface and in the interface itself between the docking model and that obtained by electron microscopy. This difference stems from the assumption in the docking study that the immunogenic loops of HRV2 and HRV1A can be superimposed in space. It can be seen in the electron microscope model that both loops start and finish at similar positions but diverge considerably in their position as they loop out of the capsid surface (Figure 6C). This divergence is not surprising since there is no sequence homology at all between the two loops and there is no cross-reactivity of 8F5 with HRV1A.

Comparison of the neutralization behaviour of mAb 8F5 towards HRV2 and mAb 17-IA towards HRV14

Both mAbs 8F5 and 17-IA neutralize a human rhinovirus and are bound bivalently. However, 17-IA is a very strong and 8F5 a very weak neutralizing agent. Why is this so? The mAbs 8F5 and 17-IA bind to different immunogenic sites: 17-IA binds to NIm-1A and obscures the canyon; mAb 8F5 binds to immunogenic site B (equivalent to NIm-II on HRV14) and does not obscure the canyon. It is thus not surprising that both the IgG 17-IA and Fab 17-IA inhibit receptor binding. IgG 8F5 does not inhibit receptor binding so apparently the receptor recognition site is not obscured by 8F5. Both IgG 17-IA and Fab17-IA exhibit strong affinity for HRV14, while the affinity of Fab 8F5 is low enough to preclude formation of defined complexes with HRV2 (see above). These differences in affinity are reflected in the difference of the epitopes; 8F5 binds to an essentially contiguous epitope while 17-IA binds to a very large epitope with several framework residues being involved in contacts with the viral surface.

A comparison of the orientation of the Fabs with respect to the 2-fold axis reveals interesting differences [compare Figure 5A and B with Figure 3D in Smith *et al.* (1993a)]. There is a comparative rotation of these Fabs about the Fab long axis of >90°. This could be accounted for by rotational flexibility at the hinge region or by differences in the way the Fabs are linked to the Fc. Knowledge of the sequences at the hinge region may lead to an understanding of these differences. Very high rotational flexibility of Fabs with respect to the Fc have previously been observed in the case of an mAb bound to tetrameric haemacyanin (Wade *et al.* 1989). The large difference in binding geometry raises the question as to what determines monovalent or bivalent attachment.

Inhibition of viral uncoating (by cross-linking of the capsid pentamers) has been proposed as a secondary mechanism of neutralization by 17-IA and may be hypothesized to be the primary mechanism of neutralization for 8F5. HRV2 and HRV14 belong to the minor and major receptor groups respectively, but this is unlikely to be an important factor in determining the main neutralization mechanism. However, as the receptor binding sites are probably not identical, any given antigenic site will not evoke exactly the same neutralizing mechanisms. In a study of 32 HRV14-neutralizing mAbs (Mosser *et al.*, 1989) the 10 mAbs classified as strong neutralizers all bound to NIm-IA thus potentially inhibiting receptor binding. In contrast, in a similar study of 14 HRV2 neutralizing mAbs (Appleyard *et al.*, 1990) the three strongest neutralizers bound to the B site (NIm-II equivalent). This type of comparison is unfortunately biased by the difficulty in obtaining a really representative selection of mAbs. In the HRV2 study only one mAb directed against the A site (NIm-1 equivalent) was studied.

It will be recalled that while the receptor binding site for HRV14 is known to be in the 'canyon', the receptor site for HRV2 has not yet been identified. The 'dimple' (a small depression) on the icosahedral 2-fold axis has a highly conserved sequence within minor group HRV (Chapman and Rossmann, 1993) and thus may be considered a potential receptor site. However, since the 8F5 obscures the 'dimple' but does not inhibit receptor binding, this tends to eliminate it as a potential receptor-binding site in favour of a site in the 'canyon'.

In summary, the differences between mAbs 17-IA and 8F5 are as follows. mAb 17-IA has a more extended epitope and binds more strongly to HRV14 than mAb 8F5 binds to HRV2. By virtue of its binding site, mAb 17-IA probably invokes at least two mechanisms of neutralization: inhibition of receptor binding and inhibition of virus uncoating. 8F5 binds less strongly to its cognate HRV and due to the topology of its binding site probably invokes only one mechanism of neutralization: inhibition of virus uncoating. Whatever mechanism of neutralization is involved, the affinity of the mAb for its HRV must be an important factor in the neutralization efficiency of the mAb.

From this study it is apparent that bivalent binding of an mAb to HRV is possible for a smaller spanning distance than was previously considered possible and that bivalent binding does not ensure strong neutralization.

Materials and methods

Preparation and purification of HRV2, mAb 8F5 and Fab 8F5

HRV2 was prepared essentially as described by Skern *et al.* (1984) with the exception that the virus pellet obtained from the polyethylene glycol precipitation was treated with 0.3 mg/ml trypsin for 5 min at 37°C (Kim *et al.*, 1989). The solution was then made 0.07% in *N*-laurylsarcosine and the virus was purified by sucrose gradient centrifugation. Preparation and purification of mAb 8F5 and its Fab have been described previously (Tormo *et al.*, 1990).

Preparation of HRV2/8F5 complexes

HRV2 (25 μg) and mAb-8F5 were incubated at a molar ratio of 1:100 in 50 μl of incubation buffer (50 mM Tris–HCl, 150 mM NaCl, 2 mM $CaCl_2$, 30 mM $MgCl_2$, pH 7.4) for 1 h at room temperature. Decreasing the molar ratio to 1:300 or incubating at 4°C overnight did not apparently change the complex formation. Excess mAb was removed by passage through a Sephacryl S300 Spun column (Pharmacia) which had been equilibrated with incubation buffer. Assuming no loss of HRV2, the complex was estimated to have a total protein concentration of 1 μg/μl so additional specimen concentration was not necessary. The total time for purification with a spun column was only 3 min thus minimizing the loss of mAb from the complex during purification. The HRV2/Fab-8F5 complex was prepared exactly as for the HRV2/mAb-8F5 complex but with a molar ratio of from 1:200 to 1:600.

Preparation of frozen hydrated specimens

Frozen hydrated specimens were prepared on holey carbon grids as previously described (Hewat *et al.*, 1992a,b). The holey carbon film supported on 400 mesh grids was not glow discharged before use. Samples of the virus suspension (4 μl) were applied to grids, blotted immediately with filter paper for 1–2 s and rapidly plunged into liquid ethane cooled by nitrogen gas at –175°C. Specimens were photographed at a temperature of close to –180°C using a Gatan 626 cryo-holder in a Phillips CM200 operating at 200 kV. Images were obtained under low-dose conditions (<10e/Å^2) at a nominal magnification of ×27 500 at 1.5, 2.0 and 3.0 μm underfocus.

Image analysis

Preliminary selection of micrographs, digitization and preparation of virus particle images for analysis were performed as described previously (Hewat *et al.*, 1992a). The pixel size of 10.5 μm on the micrograph corresponds to a nominal pixel size of 3.80 Å/pixel at the specimen. Further image analysis was performed on a DEC Alpha using modified versions of the MRC icosahedral programs supplied by S.Fuller (Fuller, 1987). The orientations and origins of each particle were determined and refined by the method of common lines (Crowther, 1971). Of 175 particles analysed, 52 particles were retained from an image at 3.3 μm defocus to give a reconstruction including information to 29 Å resolution. For this data set all inverse eigenvalues were <0.1. The high rejection rate was probably partially due to a variable occupancy of the mAb and the presence of 30 disordered Fc domains which contribute to the noise. Images in the same focal series closer to focus were analysed using the orientations determined at the highest defocus as starting data. The best reconstruction used 32 particles and included information to 25 Å resolution. The phase residual went to 90° at 23 Å^{-1} but the resolution was restricted to 25 Å because of insufficient coverage of all orientations. There was a preferred orientation of around $\theta = 82°$, $\psi = 20°$. All the inverse eigenvalues were <1.0 and 99.5% were <0.1. Isosurface representations of the reconstructed density were visualized using Explorer on an SGI.

Fitting the HRV1A and Fab 8F5 X-ray structures to the cryo-electron microscope reconstructed density

First, the cryo-electron microscope reconstructed density map of the HRV2/mAb-8F5 complex was scaled to the X-ray data by comparing the HRV capsid density only. The radially averaged density within a spherical shell from a radius of 115–145 Å was compared by cross-correlation. This gave a pixel size of 3.55 (± 0.2) Å/pixel. This is to be compared with a previous calibration of 3.67 Å/pixel using TMV. Secondly, a correction for the effect of the CTF on the cryo-electron microscopy reconstruction was estimated by comparing the cryo-electron microscope density map of HRV2/Fab-8F5 (since the Fc is not visible) with the density <105 Å (corresponding to the viral RNA) removed and the X-ray docking model of the Fab 8F5 on HRV1A (Tormo *et al.*, 1995). The Fourier transform of identical projections of both maps were compared and their ratio gave a radial CTF correction for the electron microscope images. The X-ray structure of Fab 8F5 was then fitted by eye to the electron microscope density using the program 'O' on an SGI. The new coordinates of the Fab were output from 'O' and a low resolution density map calculated by considering only the C_α with a weighting corresponding to the relative molecular mass of the corresponding amino acid residue. The density of one Fab was extracted from the electron microscope density map for comparison by cross-correlation of all sections along each Cartesian axes in real space with the program Semper6 running on an SGI. An improved fit position for the X-ray Fab was estimated and applied to the X-ray Fab coordinates in 'O'. This refinement cycle was repeated several times giving a best fit to within one pixel. The initial fit by eye was remarkably close to the final fit; the greatest movement of any part of the Fab was <2 pixels in one direction.

Acknowledgements

We wish to thank M.Hilpert and R.Wandl for preparing the purified HRV2, 8F5 and Fab 8F5, A.Ellinger for help with characterizing the samples, S.Fuller for helpful advice and supplying his latest versions of the MRC icosahedral programs, I.Fita for supplying the docked co-ordinates of HRV2 on 8F5 and icosahedral symmetry generation programs, J.-Y.Sgro for supplying the roadmap of HRV1A, J.-P.Eynard and F.Metoz for assistance in running the computers, E.Pebay-Peyroula and colleagues for advice on using the crystallographic programs and R.H.Wade for discussions. This work was supported in part by the Austrian Science Foundation (grant # P09999-MOB to D.B.).

References

Appleyard,G., Russell,S.M., Clarke,B.E., Speller,S.A., Trowbridge,M. and Vadolas,J. (1990) *J. Gen. Virol.*, **71**, 1275–1282.
Chapman,M.S. and Rossmann,M.G. (1993) *Virology*, **195**, 745–756.
Crowther,R.A. (1971) *Phil. Trans. R. Soc. Lond.*, **B 261**, 221–230.
Duechler,M., Ketter,S., Skern,T., Kuechler,E. and Blaas,D. (1993) *J. Gen. Virol.*, **74**, 2287–2291.
Fuller,S.D. (1987) *Cell*, **48**, 923–934.
Greve,J.M., Davis,G., Meyer,A.M., Forte,C.P., Yost,S.C., Marlor,C.W., Kamarck,M.E. and McClelland,A. (1989) *Cell*, **56**, 839–847.
Hewat,E.A., Booth,T.F., Loudon,P.T. and Roy,P. (1992a) *Virology*, **189**, 10–20.
Hewat,E.A., Booth,T.F. and Roy,P. (1992b) *J. Struct. Biol.*, **109**, 61–69.
Hofer,F., Gruenberger,M., Kowalski,H., Machat,H., Huettinger,M., Kuechler,E. and Blaas,D. (1994) *Proc. Natl Acad. Sci. USA*, **91**, 1839–1842.
Kim,S. *et al.* (1989) *J. Mol. Biol.*, **210**, 91–111.
Liu,H., Smith,T.J., Lee,W.M., Mosser,A.G., Rueckert,R.R., Olson,N.H., Cheng,R.H. and Baker,T.S. (1994) *J. Mol. Biol.*, **240**, 127–137.
Mosser,A.G., Leippe,D.M. and Rueckert,R.R. (1989) In Semler,B.L. and Ehrenfeld,E. (eds), *Molecular Aspects of Picornavirus Infection and Detection.* American Society for Microbiology, Washington DC, Vol. I, pp. 155–167.
Oliveira,M.A. *et al.* (1993) *Structure*, **1**, 51–68.
Olson,N.H., Kolatkar,P.R., Oliveira,M.A., Cheng,R.H., Greve,J.M., McClelland,A., Baker,T.S. and Rossmann,M.G. (1993) *Proc. Natl Acad. Sci. USA*, **90**, 507–511.
Porta,C., Wang,G., Cheng,H., Chen,Z., Baker,T.S. and Johnson,J.E. (1994) *Virology*, **204**, 777–788.
Prasad,B.V., Burns,J.W., Marietta,E., Estes,M.K. and Chiu,W. (1990) *Nature*, **343**, 476–479.
Rossmann,M.G. (1989) *J. Biol. Chem.*, **264**, 14587–14590.
Rossmann,M.G. and Johnson,J.E. (1989) *Annu. Rev. Biochem.*, **58**, 533–573.
Rossmann,M.G. *et al.* (1985) *Nature*, **317**, 145–153.
Sherry,B., Mosser,A.G., Colonno,J.R. and Rueckert,R.R. (1985) *J. Virol.*, **57**, 246–257.
Skern,T., Sommergruber,W., Blaas,D., Pieler,C. and Kuechler,E. (1984) *Virology*, **136**, 125–132.
Skern,T., Neubauer,C., Frasel,L., Gruendler,P., Sommergruber,W., Zorn,W., Kuechler,E. and Blaas,D. (1987) *J. Gen. Virol.*, **68**, 315–323.
Smith,T.J., Olson,N.H., Cheng,R.H., Chase,E.S. and Baker,T.S. (1993a) *Proc. Natl Acad. Sci. USA*, **90**, 7015–7018.
Smith,T.J. *et al.* (1993b) *J. Virol.*, **67**, 1148–1158.
Staunton,D.E., Merluzzi,V.J., Rothlein,R., Barton,R., Marlin,S.D. and Springer,T.A. (1989) *Cell*, **56**, 849–853.

Tomassini,E., Graham,T., DeWitt,C., Lineberger,D., Rodkey,J. and Colonno,R. (1989) *Proc. Natl Acad. Sci. USA*, **86**, 4907–4911.
Tormo,J., Fita,I., Kanzler,O. and Blaas,D. (1990) *J. Biol. Chem.*, **265**, 16799–16800.
Tormo,J., Stadler,E., Skern,T., Auer,H., Kanzler,O., Betzel,C., Blaas,D. and Fita,I. (1992) *Protein Sci.*, **1**, 1154–1161.
Tormo,J., Blaas,D., Parry,N.R., Rowlands,D., Stuart,D. and Fita,I. (1994) *EMBO J.*, **13**, 2247–2256.
Tormo,J., Centeno,N.B., Fontana,E., Bubendorfer,T., Fita,I. and Blaas,D. (1995) *Proteins*, **23**, 491–501.
Trus,B.L., Newcomb,W.W., Booy,F.P., Brown,J.C. and Steven,A.C. (1992) *Proc. Natl Acad. Sci. USA*, **89**, 11508–11512.
Wade,R.H., Taveau,J.C. and Lamy,J.N. (1989) *J. Mol. Biol.*, **206**, 349–356.
Wang,G.J., Porta,C., Chen,Z.G., Baker,T.S. and Johnson,J.E. (1992) *Nature*, **355**, 275–278.
Wein,M.W., Filman,D.J., Stura,E.A., Guillot,S., Delpeyroux,F., Crainic,R. and Hogle,J.M. (1995) *Struct. Biol.*, **2**, 232–243.
Wikoff,W.R., Wang,G.J., Parrish,C.R., Cheng,R.H., Strassheim,M.L., Baker,T.S. and Rossmann,M.G. (1994) *Structure*, **2**, 595–607.

Received on October 25, 1995; revised on November 28, 1995